Electronic Supplementary Material (ESI) for Nanoscale.


*Supporting Information*

# Core–Satellite–Satellite Hierarchical Nanostructures: Assembly, Plasmon Coupling, and Gap-Selective Surface-Enhanced Raman Scattering

Hoa Duc Trinh, Seokheon Kim, Joohwan Park, and Sangwoon Yoon*

Department of Chemistry, Chung-Ang University,
84 Heukseok-ro, Dongjak-gu, Seoul 06974, Korea.

*E-mail: sangwoon@cau.ac.kr

# 1. Experimental Method

## 1.1 Materials

Trisodium citrate ($C_6H_5Na_3O_7 \cdot 2H_2O$, ≥99.0%), gold(III) chloride ($HAuCl_4 \cdot 3H_2O$, ≥99.9%), RBS 35 solution, methanol (≥99.8%), (3-aminopropyl)trimethoxysilane (APTMS, 97.0%), NaOH (≥98.0%), 1,8-octanedithiol (C8DT, ≥97.0%), 4-aminobenzenethiol (ABT, ≥97.0%), and 1,4-benzenedimethanethiol (BDMT, 98.0%) were purchased from Sigma-Aldrich. HCl (35.0–37.0%) and ethanol (≥99.9%) were purchased from Duksan Chemical. All chemicals were used as received without further purification. $N_2$ was purchased from Air Korea. Microscope slides (1 mm thickness) were purchased from Marienfeld and then cut into 25 × 13 $mm^2$ pieces. All solutions were freshly prepared prior to use. Ultrapure water (HPLC grade, J. T. Baker) was used for all aqueous solutions.

## 1.2 Synthesis of AuNPs

***Core and Sat1 AuNPs*:** Citrate-capped AuNPs with a diameter of approximately 70 or 32 nm were synthesized using the seeded growth method.[1] Briefly, aqueous stock solutions of trisodium citrate (60 mM) and gold(III) chloride (25 mM) were freshly prepared. **Table 1** summarizes the input volume of water, trisodium citrate, and gold(III) chloride solutions used in every step. **Step (1):** Water was boiled under vigorous stirring in a three-necked round-bottom flask using a heating mantle. A condenser was used to prevent water evaporation. When the water temperature reached 100 °C, a trisodium citrate solution was added. After 5 min, a gold(III) chloride solution was injected. The mixture was stirred at 100 °C for 30 min and then cooled to 90 °C. **Step (2):** A gold(III) chloride solution was injected into the above solution. Then, another gold(III) chloride solution was injected again after 30 min. The reaction was allowed to react for a further 30 min. **Step (3):** The above solution was diluted by adding water. Once the temperature reached 90 °C again, a trisodium citrate solution was added. After 5 min, another gold(III) chloride solution was added to the mixture. Subsequently, an additional of gold(III) chloride solution was injected after 30 min. The reaction was allowed to proceed for 30 min. Step (3) was repeated until the UV–vis extinction peak appeared at 542 or 527 nm. One aliquot (1 mL) was extracted at every growth step for UV–vis and transmission electron microscopy (TEM) characterization.

**Table 1.** Input volume of solvents and reagents for synthesizing citrate-capped AuNPs using a seeded growth method.

| Seeded growth steps | | Core (70 nm) | Sat1 (32 nm) |
|---|---|---|---|
| **Step (1)** | Water | 150 mL | 600 mL |
| | Trisodium citrate | 6 mL | 24 mL |
| | Gold(III) chloride | 1 mL | 4 mL |
| **Step (2)** | Water | 0 | 0 |
| | Trisodium citrate | 0 | 0 |
| | Gold(III) chloride | 1 + 1 mL | 4 + 4 mL |
| **Step (3)** | Water | 150 mL | 300 mL |
| | Trisodium citrate | 6 mL | 12 mL |
| | Gold(III) chloride | 3 + 3 mL | 4 + 4 mL |
| **Step (4)** | Water | 300 mL | |
| | Trisodium citrate | 6 mL | |
| | Gold(III) chloride | 3 + 3 mL | |
| **Step (5)** | Water | 300 mL | |
| | Trisodium citrate | 6 mL | |
| | Gold(III) chloride | 3 + 3 mL | |
| **Step (6)** | Water | 0 | |
| | Trisodium citrate | 6 mL | |
| | Gold(III) chloride | 3 + 3 mL | |
| **Step (7)** | Water | 0 | |
| | Trisodium citrate | 6 mL | |
| | Gold(III) chloride | 3 + 3 mL | |

***Sat2 AuNPs*:** Citrate-capped AuNPs with a diameter of approximately 20 nm were synthesized using the Turkevich method.[2] Briefly, 950 mL of a 1.8 mM trisodium citrate aqueous solution was boiled under vigorous stirring in a 1 L three-necked round-bottom flask with a heating mantle. A condenser was utilized to prevent water evaporation. After reaching 100 °C, 50 mL of a 5 mM gold(III) chloride aqueous solution was injected into the solution. The reaction proceeded for 30 min and then was cooled to room temperature. One aliquot of 1 mL was extracted for UV–vis and TEM characterization.

### 1.3 Characterization

***UV-vis spectroscopy*:** Optical properties of the synthesized AuNPs were measured using a UV-vis spectrometer (Lambda 25, PerkinElmer). The localized surface plasmon band (LSPR) appears near 530 nm in the extinction spectra (**Figure S1**). The peak position red-shifts as the AuNP size increases, as the Mie theory predicts.[3] The concentration of the AuNP solutions was determined from the UV-vis spectra, following the method developed by Haiss *et al.*[4]

***TEM***: The size of the AuNPs was determined using TEM (JEM-F200, Jeol) images and ImageJ software. The samples for TEM were prepared by dropping a 5 µL of citrate-capped AuNP solution onto carbon-coated copper grids, followed by drying under ambient air.

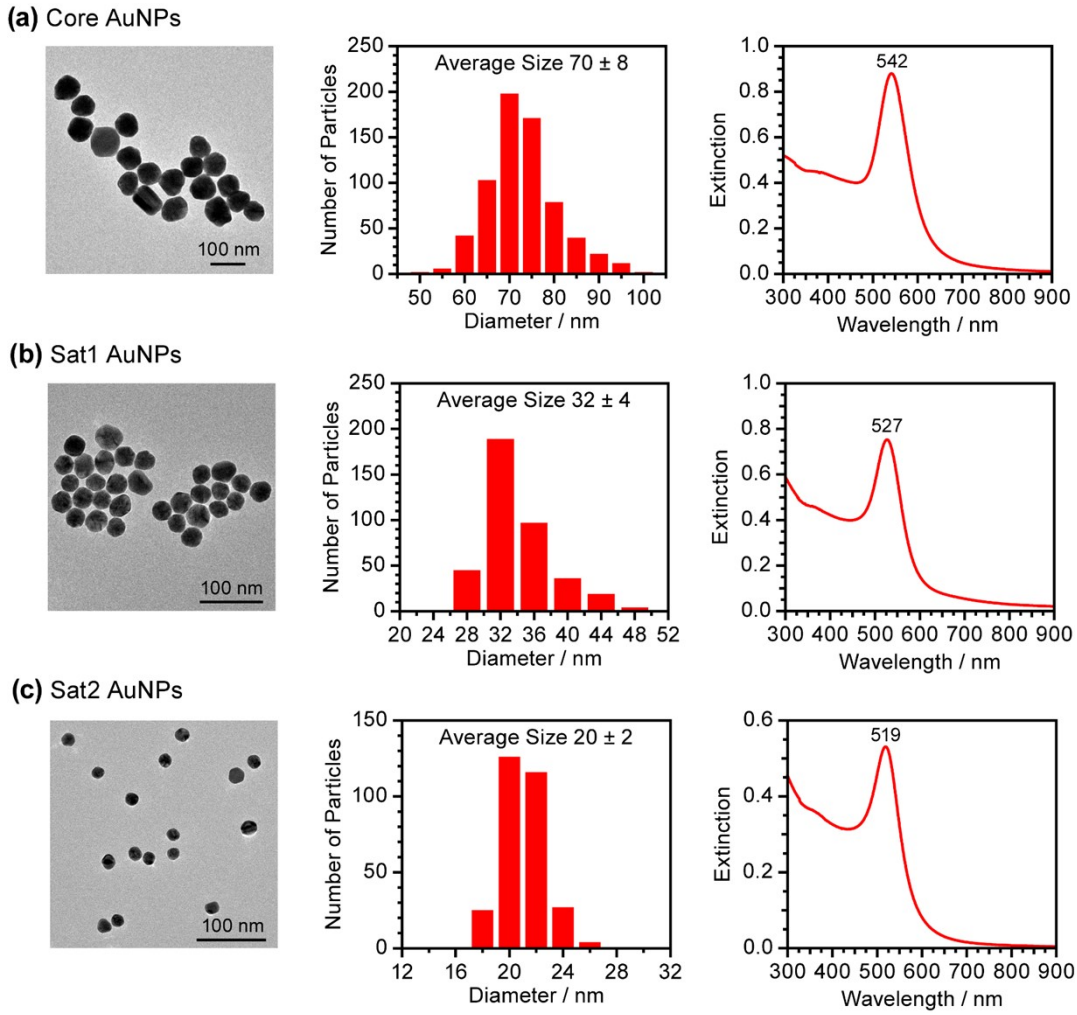


**Figure S1.** Representative TEM images, size distribution, and UV–vis spectra of (a) core, (b) Sat1, and (c) Sat2 AuNPs.

### 1.4 Assembly

The core-satellite-satellite (CSS) assembly process was based on the previously reported dimer assembly method.[5] **Step (1)**: A glass slide was cleaned by dipping in a 15% RBS detergent solution at 90 °C for 5 min and then sonicated in water for another 5 min. The cleaned glass slide was thoroughly rinsed with water and immersed in a 1:1 (v/v) methanol and HCl mixture for 30 min. Then, the glass slide was washed with water, blow-dried with $N_2$, and then left to completely dry in an oven at 100 °C for 2 h. Subsequently, the surfaces of the glass slide were modified with amines; the entire glass slide was immersed in a 1% APTMS ethanolic solution for 30 min. Then, the amine-functionalized glass slide was sonicated in ethanol for 5 min, rinsed with ethanol, blow-dried with $N_2$, and then placed in an oven at 125

°C for 3 h. **Step (2)**: The amine-functionalized glass slide was fully immersed in a citrate-capped 70 nm Core AuNP solution (23 pM) for 5 h. The Core AuNPs were adsorbed onto the glass slide surfaces by electrostatic interactions. The unbound AuNPs were removed by carefully washing with ethanol. **Step (3)**: The entire substrate was immersed in an aqueous NaOH solution (50 mM) for 5 h to remove unreacted amines. This step was performed to prevent satellite AuNPs from adsorbing onto the amines on the glass surfaces in subsequent steps. Then, the substrate was carefully cleaned with ethanol to avoid the removal of the adsorbed Core AuNPs. **Step (4)**: Linker1 was attached on the Core AuNP surfaces by immersing the Core-adsorbed glass substrate in a Linker1 ethanolic solution (1 mM) for 1 h. Ethanol was used to wash off all the excess linker molecules. **Step (5)**: The Linker1-functionalized Core AuNPs on the glass substrate were immersed in a Sat1 AuNP solution (214 pM) for 6 h to form the CS structure. The unbound Sat1 AuNPs were removed by washing with ethanol. **Step (6)**: Linker2 was attached to the Sat1 AuNP surfaces by immersing the entire substrate in a Linker2 ethanolic solution (1 mM) for 1 h. Since Linker1 fully covered the Core AuNP surfaces, Linker2 was attached only to the Sat1 AuNP surfaces. The excess linker molecules were removed by washing with ethanol. **Step (7)**: The CSS assembly was completed by immersing the Linker2-functionalized CS particles on the glass substrate in a Sat2 AuNP solution (710 pM) for 4 h. The unbound Sat2 AuNPs were removed by washing with ethanol.

Our assembly method is extremely reproducible as the SEM images indicate (*vide infra*). We would evaluate that the success rate is ~95%, meaning that in most cases, we were able to make the CSS nanoassemblies without any problems. The yield was also very high. The entire glass slides were covered with the CSS nanoassemblies. The uniformity of the distribution and yield can be judged by the even color across the glass slide as shown in Figure 2b in the main manuscript.

The most challenging part is to maintain the quality of chemicals. Fresh and high purity chemicals are always recommended. The quality of APTMS and NaOH determines the silanization and desilanization of glass slides. NaOH often absorbs moisture unless properly kept. Dithols are oxidized to disulfides over time. Another challenging part is to endure the laborious stepwise process for assembly. It takes at least 24 h to complete the assembly process. The successful assembly requires careful washing and rinsing between the steps. We recently developed a new technique where a use of plasma significantly shortens the assembly process. The results will be published in near future.

### 1.5 Measurements

***Scanning electron microscopy (SEM)***: The assembly structures were measured using a SEM (Sigma, Carl Zeiss).

***UV-vis spectroscopy***: The optical responses of the prepared CS or CSS nanoassemblies were measured using a UV–vis spectrometer. For the nanoparticles adsorbed on the glass slides, the entire substrate was placed in a quartz cuvette in the presence of ethanol.

***Raman spectroscopy***: We compared the plasmon-induced electric field intensities between Gap1 and Gap2 using surface-enhanced Raman spectroscopy (SERS). We prepared CS or CSS nanoassemblies where the ABT molecules (Raman probe) were positioned in desired nanogaps. Note that other gaps were filled with C8DT that is invisible in Raman spectra (see Sec. 5 below). Raman spectra were acquired using a microscope (DM, Leica), combined with a laser (LM-785, Ondax) and a spectrometer (RamanRxn1, Kaiser Optical Systems). The sample on a glass slide was placed under a microscope objective (50×, N.A. 0.75, Leica). The laser at 785 nm was focused onto the sample through the objective. The laser spot size was 10 μm. The power of the laser at the sample was measured at 10 mW. The Raman scattering light was collected by the same objective and transmitted to the spectrometer, equipped with two notch filters, transmissive holographic grating (resolution 5 $cm^{-1}$), and a CCD. Raman spectra were acquired at a total exposure time of 3 s. A glass substrate Raman spectrum was subtracted for the samples prepared on the glass substrate.

Not only the electric field strength of nanogaps, but also the number of nanoassemblies within the focus of the laser contributes to the ensemble SERS intensities. To account for this, we correlated the SERS intensities to the number of nanoassemblies as illustrated in Figure 5a. We placed a 50-mesh finder grid (G50-C3, Gilder Grids) that consists of 420 × 420 $\mu m^2$ square holes on a sample slide. Then, we acquired Raman spectra from the center area of each randomly selected five grid cells. Subsequently, we obtained SEM images (14 × 9 $\mu m^2$) from the same five spots. The density of particles was calculated. Dividing the SERS intensity at 1586 $cm^{-1}$ ($\nu_{CC}$ of ABT) by the number of nanoassemblies within the laser focal area (10 μm) for each position, followed by the averaging, yields the SERS intensity per particle for the specific type of CS or CSS nanoassembly structure. Then, we repeated the experiments on four or five independently prepared samples. Averaging the four or five results gives the final SERS intensity per particle for the corresponding nanoassembly, presented in Figure 5b.

**1.6 Simulations**

Resonance cross-sections, charge density, and electric field distributions were calculated using a finite-difference time-domain (FDTD) software package (Lumerical Solutions). We adopted the dielectric constant for Au from Johnson and Christy.[6] The medium (ethanol) refractive index was set to 1.36. CS and CSS nanoassemblies were constructed for the calculations using spherical AuNPs with diameters of 70, 32, and 20 nm, as illustrated in Figure 3a. The gap distance was set to be 1.3 nm to emulate the self-assembled monolayer height of C8DT. The simulation parameters include 1500 nm × 1500 nm × 1500 nm for a simulation region enclosed by perfectly matched layer (PML) boundaries, 1000 fs simulation time, and a 175 nm × 175 nm × 125 nm override region with an increment of 0.5 nm mesh size. The optical responses were calculated using the total field-scattered field (TFSF) source (λ = 400–1000 nm) that propagates from the top with polarization parallel to the meridian cross-section of

the nanoassembly structure, as shown in Figure 3a. The charge density and electric field distribution were calculated at the resonance wavelengths.

## 2. CSS Images

**(a)** CSS (ABT-ABT)

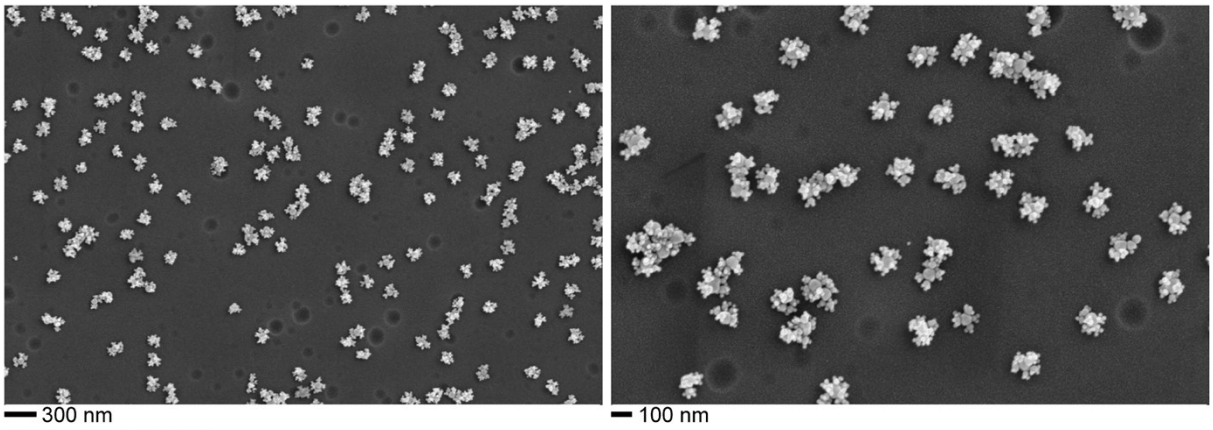


**(b)** CSS (ABT-C8DT)

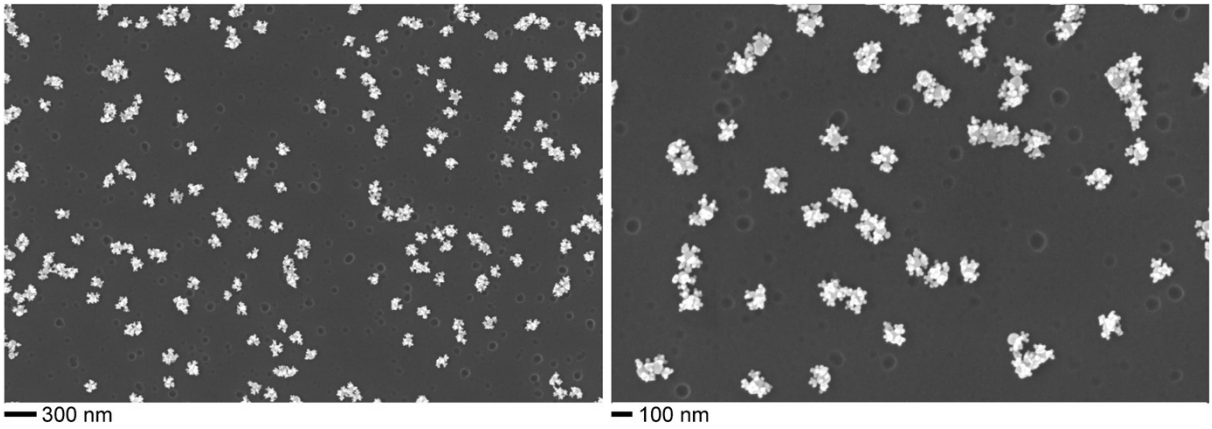


**(c)** CSS (C8DT-C8DT)

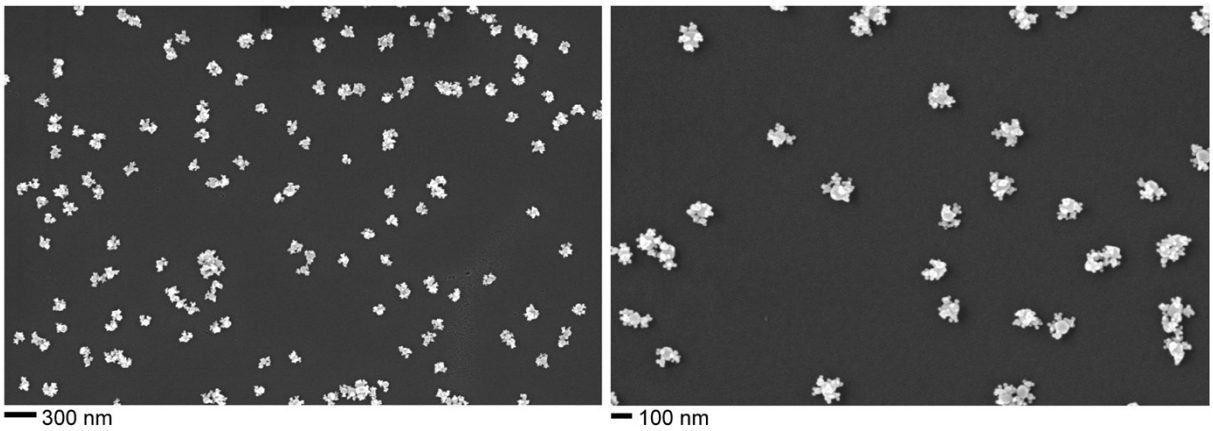

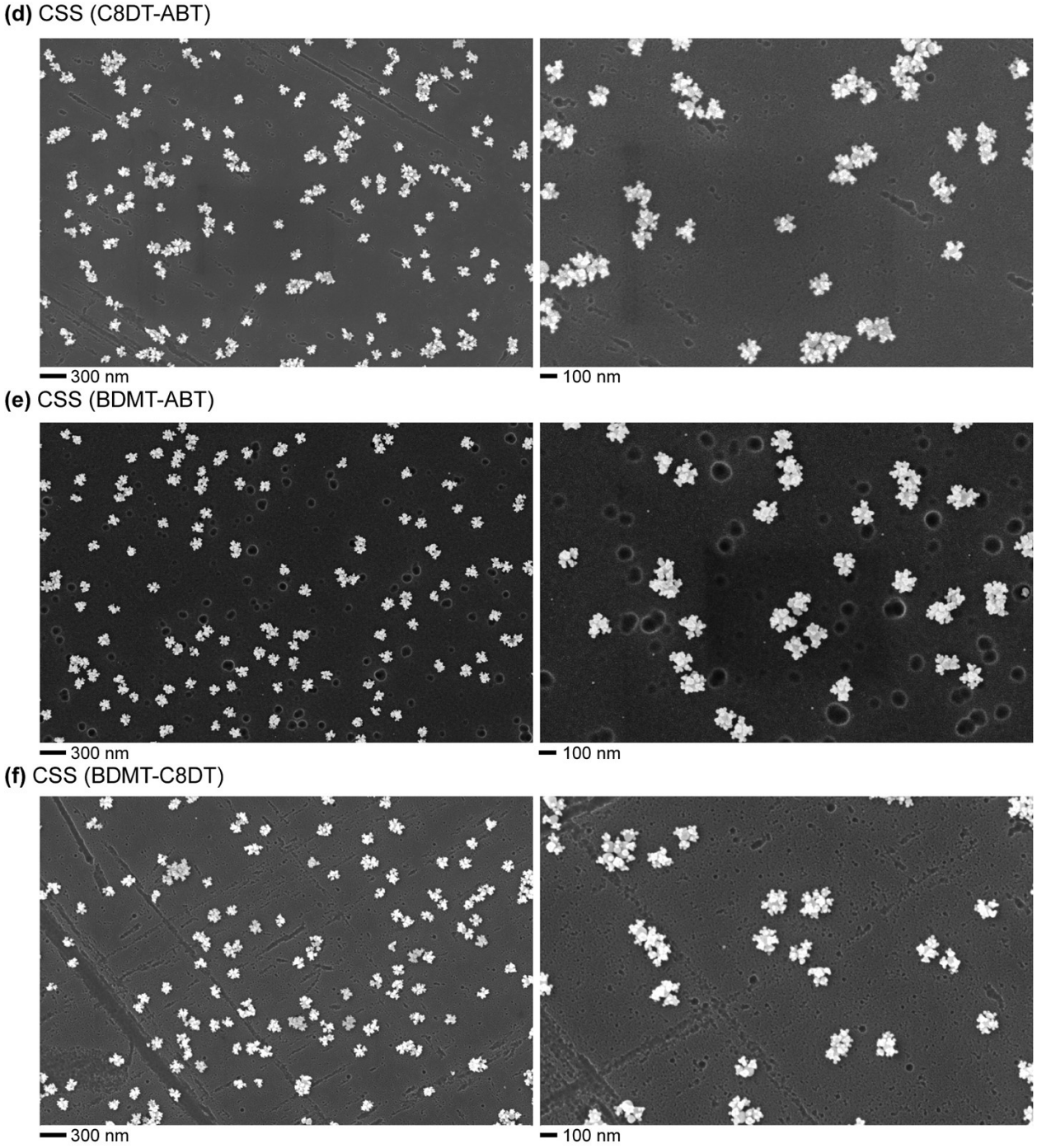


**Figure S2.** Gallery of SEM images of CSS with (Linker1–Linker2).

## 3. Radiant Coupling Mode vs. *Di–Di–Di* Coupling Mode

Our FDTD calculations of the charge density distribution reveal that the plasmon coupling scheme in CSS differs slightly from the radiant or nonradiant coupling scheme proposed by Kuttner and coworkers for CS nanostructures.[7,8] In the radiant coupling model, the largest Core AuNP interacts strongly with light and forms a plasmon dipole mode. The plasmon dipoles of the Sat1 AuNPs then align in a radial direction so that their charges interact with the local charges of the Core AuNP and become stabilized (Figure S3, left panel). Subsequently, Sat2 AuNPs interact with Sat1 AuNPs similarly, repeating the coupling between the Core and Sat1 AuNPs. Contrary to this model, our calculations show that the global and long-range dipole–dipole interactions between Sat1 or Sat2 AuNPs and Core AuNPs are more important in the *Di–Di–Di* coupling mode than the local charge–dipole interactions. The right panel in Figure S3 shows that the plasmon dipoles of the Sat1 and Sat2 AuNPs rotate counterclockwise from the radial direction such that the plasmon dipoles compensate for the dipole of the Core AuNPs.

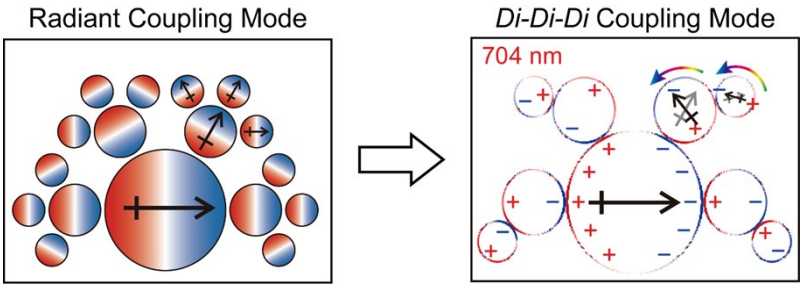


**Figure S3.** Calculated charge density distribution of the *Di–Di–Di* plasmon coupling mode of CSS (right panel) in comparison with the radiant coupling mode (left panel). In the radiant coupling scheme, the plasmon dipoles of the Sat1 and Sat2 AuNPs align in a radial direction such that they interact with the local charges of the Core and Sat1 AuNPs, respectively (left panel). In contrast, the plasmon dipoles of the Sat1 and Sat2 AuNPs rotate counterclockwise such that they are lined up with respect to the global dipole of the Core AuNPs in the *Di–Di–Di* coupling scheme (right panel).

## 4. Comparison of Binding Forces between Electrostatic Interaction and Covalent Bonding

Electrostatic interaction is weaker than covalent bonding. Citrate-capped AuNPs bind to the terminal groups of the ABT and C8DT linkers in a different fashion. ABT interacts with citrates on AuNP surfaces through the electrostatic attraction between the ammonium terminal group of ABT and the carboxylate of the citrate. On the other hand, C8DT forms an Au–S covalent bond directly with the AuNP surfaces by displacing the citrates.

In the following experiments, we assembled CS nanostructures with ABT and C8DT linkers on glass slides and desorbed the CS nanoassemblies from the glass slides using ultrasonication. The changes in the UV–vis spectrum of the CS with ABT linkers after sonication indicate that some of the satellite AuNPs detached from the ABT linkers. In contrast, the UV–vis spectrum remains unchanged after sonication for the CS nanoassemblies linked by C8DT. This result suggests that the C8DT linkage is significantly stronger than the ABT linkage. The weaker electrostatic linkage for ABT results in variations in the nanogap distances, which broaden the plasmon coupling bands for CS. The solidly defined nanogaps by the covalent bonding of C8DT lead to well-resolved plasmon coupling bands.

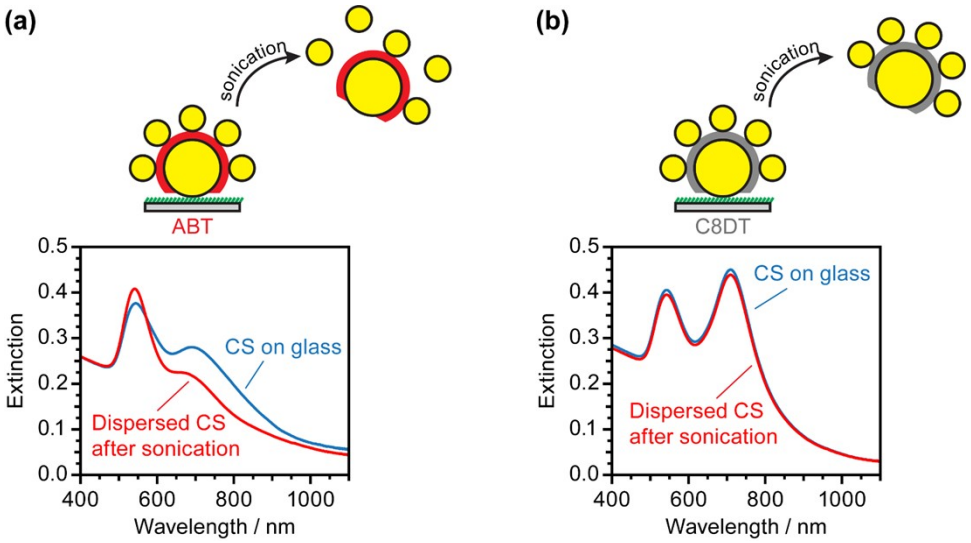


**Figure S4.** UV–vis spectra of CS nanostructures assembled by (a) ABT linkers and (b) C8DT linkers on glass slides (blue lines) and dispersed in the solution by ultrasonication (red lines). The decrease in the plasmon coupling band intensity in (a) indicates the formation of partly dissembled CS by ultrasonication.

## 5. Comparison of SERS Intensity between ABT and C8DT

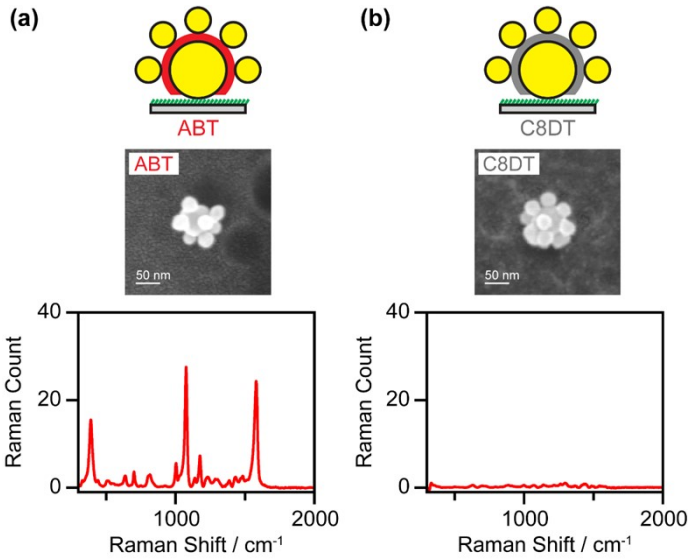


**Figure S5.** Representative SEM images and Raman spectra of CS nanostructures assembled with (a) ABT and (b) C8DT linkers. A SERS signal is observed only for the CS with ABT linkers. The considerably smaller Raman scattering cross-section of C8DT, as compared to that of ABT, makes the C8DT linkers invisible in the SERS spectra.

## 6. Calculated Scattering Spectra and Electric Field Distribution of CS and CSS

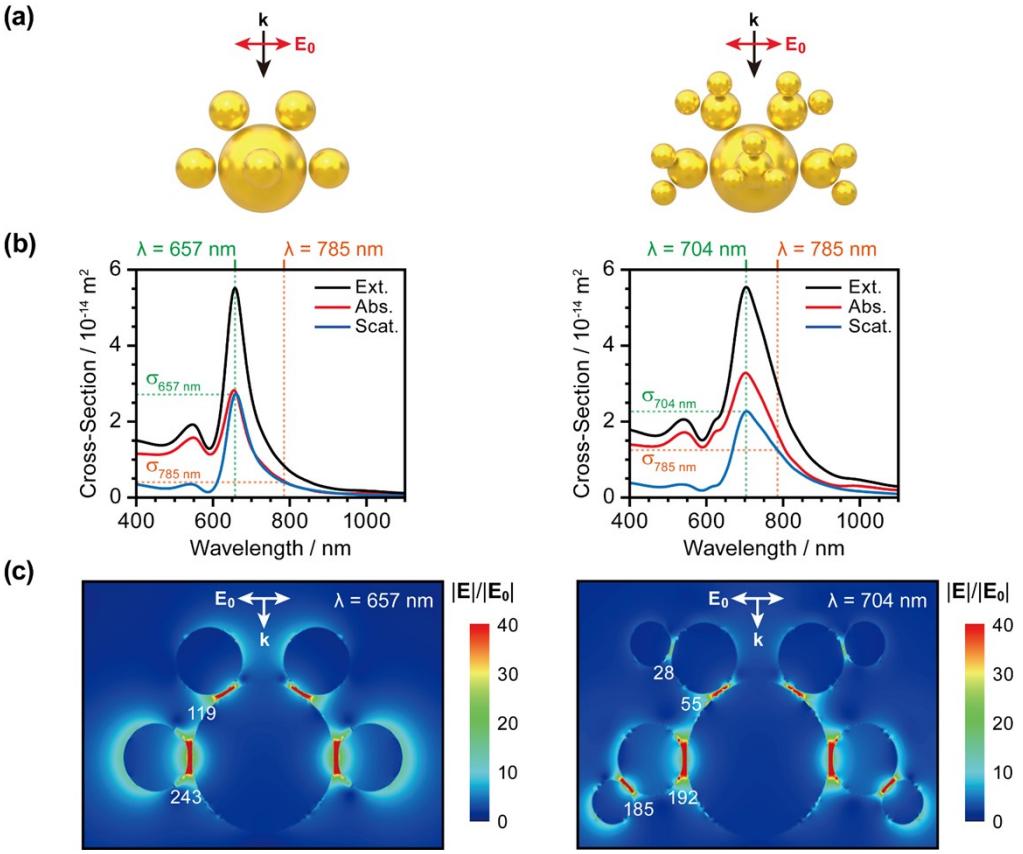


**Figure S6.** (a) Models of the CS, CSS, and incident plane wave with propagation (***k***) and polarization ($\boldsymbol{E_0}$) used for the FDTD calculations. (b) Calculated absorption (red lines), scattering (blue lines), and extinction (black lines) spectra of CS and CSS. The vertical dotted lines are drawn at the resonance wavelengths (green dotted lines) and 785 nm (red dotted lines) to compare the scattering cross-sections of CS and CSS at the corresponding wavelengths. Note that CS has a higher scattering intensity at the resonance wavelengths (657 nm for CS and 704 nm for CSS), whereas CSS has a higher scattering intensity at 785 nm. (c) Cross-sectional view of the electric field distribution in CS and CSS, induced by excitation at the corresponding resonance wavelengths. The electric field enhancement at Gap1 is higher for CS ($|\boldsymbol{E}_{max}|/|\boldsymbol{E_0}|$ = 243) than for CSS ($|\boldsymbol{E}_{max}|/|\boldsymbol{E_0}|$ = 192), presumably reflecting the scattering cross-sections at each resonance wavelength.

## 7. References


(1) Bastús, N. G.; Comenge, J.; Puntes, V., Kinetically Controlled Seeded Growth Synthesis of Citrate-Stabilized Gold Nanoparticles of up to 200 nm: Size Focusing Versus Ostwald Ripening. *Langmuir* **2011**, *27*, 11098-11105.

(2) Turkevich, J.; Stevenson, P. C.; Hillier, J., A Study of the Nucleation and Growth Processes in the Synthesis of Colloidal Gold. *Discuss. Faraday Soc.* **1951**, *11*, 55-75.

(3) Maier, S. A., *Plasmonics: Fundamentals and Applications*. Springer: New York, 2007.

(4) Haiss, W.; Thanh, N. T.; Aveyard, J.; Fernig, D. G., Determination of Size and Concentration of Gold Nanoparticles from Uv−Vis Spectra. *Anal. Chem.* **2007**, *79*, 4215-4221.

(5) Cha, H.; Yoon, J. H.; Yoon, S., Probing Quantum Plasmon Coupling Using Gold Nanoparticle Dimers with Tunable Interparticle Distances Down to the Subnanometer Range. *ACS Nano* **2014**, *8*, 8554-8563.

(6) Johnson, P. B.; Christy, R. W., Optical Constants of the Noble Metals. *Phys. Rev. B* **1972**, *6*, 4370-4379.

(7) Höller, R. P. M.; Dulle, M.; Thomä, S.; Mayer, M.; Steiner, A. M.; Förster, S.; Fery, A.; Kuttner, C.; Chanana, M., Protein-Assisted Assembly of Modular 3D Plasmonic Raspberry-Like Core/Satellite Nanoclusters: Correlation of Structure and Optical Properties. *ACS Nano* **2016**, *10*, 5740-5750.

(8) Höller, R. P. M.; Jahn, I. J.; Cialla-May, D.; Chanana, M.; Popp, J.; Fery, A.; Kuttner, C., Biomacromolecular-Assembled Nanoclusters: Key Aspects for Robust Colloidal SERS Sensing. *ACS Appl. Mater. Interfaces* **2020**, *12*, 57302-57313.